

DOI: 10.1002/adem.201400489

Parameters for Inherently Homogeneous Sintering Processes

By Friedrich Raether*

Thermodynamic criteria are introduced to calculate the driving force for the formation of heterogeneous metastable states during sintering. As already shown for one special case of liquid phase sintering, these metastable states significantly affect the reliability of sintered ceramics. Inherently safe sintering processes are proposed, providing a homogeneous evolution of microstructure. A desintering parameter is defined which can be used for a quantitative evaluation of different sintering processes in terms of their tendency for formation of heterogeneity. The desintering parameter has been calculated using sintering simulations in 3D representative volume elements. For that, a deterministic model has been developed. It considers interface energy minimization and grain growth for random arrangements of particles. Computational effort could be significantly reduced by periodic continuation of the microstructure at the sides of the RVE. Basic parameters controlling inherently homogeneous sintering are presented. Surface diffusion is positive at large dihedral angles. Unexpectedly, grain growth can be advantageous as well, provided that it acts continuously during the entire sintering cycle.

1. Introduction

Coarsening of the microstructure and grain growth is a well known phenomenon in sintering science. More than 4000 papers were published on these topics during the last 4 decades. Much less attention was paid to differential sintering: 30 papers. However, differential sintering can significantly deteriorate material properties of sintered products. Grain growth starts earlier in regions which are denser than the residual material. Also, large pores are formed between the dense regions which are difficult to eliminate in final stage sintering. Even local desintering is observed, leading to the opening of particle contacts which have already been formed, while the main part of the compact is densifying.^[1,2] The inhomogeneity caused by differential sintering leads to decrease of strength and reliability and is considered as one of the most important obstacles for a wider use of sintered parts.

Constraints affecting local shrinkage during sintering, e.g., acting during co-firing, have frequently been shown to cause differential sintering phenomena (compare, e.g., ref.^[3]). With free sintering, differential shrinkage was intensively studied by F.F. Lange since the 1980s.^[1,4-7] He showed that

inhomogeneity, which was already present in the green compact, led to differential shrinkage during sintering.^[5] However, desintering was reported even for partially sintered periodic arrays of polymer spheres^[5] and glass and copper spheres.^[2] Therefore, random arrangements of particles with a size distribution were considered favorable to avoid differential sintering.^[5] Lin and De Jonghe suggested a pre-coarsening treatment at relatively low temperatures, to decrease differential sintering effects.^[8] Since surface diffusion is usually more active at lower temperatures than densifying mechanisms, the microstructure can be stabilized by this treatment before shrinkage sets in and creates differential stresses. They showed that homogeneity of sintered compacts could be improved by the pre-coarsening process.^[8] On the other hand, a two-step sintering process was recently proposed starting at a short holding period at high temperature followed by a longer holding period at lower temperature.^[9] It was reported that this process can also lead to more homogenous microstructures.

A measure is required to discuss heterogeneity during sintering on a quantitative base. For that, the scaled variance of pore area distribution was proposed.^[10] The pore area is measured in polished sections of green or partially sintered compacts using scanning electron microscopy (SEM). For each sample, the variance σ^2 of pore area distribution is obtained from the data of several sections of the same size. Note that σ is the corresponding standard deviation of pore area

[*] Dr. F. Raether

Fraunhofer-Center for High Temperature Materials and Design, Gottlieb-Keim-Str. 60, Bayreuth 95448, Germany
E-mail: friedrich.raether@isc.fraunhofer.de

distribution. The area A of these sections is varied to investigate homogeneity on different length scales. Since σ^2 strongly decreases with area A , a simple scaling was introduced considering the variance ρ_{ran}^2 expected for a random distribution of mono-sized circles with the radius of average pore chord length l_p and average pore fraction p :

$$\sigma_{scaled}^2 = \frac{\sigma^2}{\sigma_{ran}^2} = \frac{\sigma^2 A}{p l_p^2} \quad (1)$$

It was shown that ρ_{scaled}^2 drastically increased during solid state sintering of alumina.^[10] An alternative measure for heterogeneity is the density variation in small test volumes obtained from microfocus computer tomography (μ CT).^[11,12] Whereas the strength of the SEM-based method is the measurement of short-range disorder on the submicron and micron scale, μ CT and CT are favorable for larger scales from some tens of microns up to centimeters.

The minimization of Gibbs free energy G during sintering at ambient pressure is mainly driven by decrease of interface energy – provided that no chemical reactions between the constituents occur.^[13] Application of thermodynamic principles to sintering studies was restricted to relatively simple geometries and/or special topics. Kellett and Lange used a thermodynamic approach to describe neck formation and pore elimination for different dihedral angles in the initial respectively final sintering stage.^[6,7] Exner used a simple numerical model to study the effect of grain boundary and surface diffusion on equilibrium shape during sintering.^[14] Delannay presented an average Voronoi cell and sophisticated analytical solutions to study equilibrium shapes in a wider portion of the sintering cycle.^[15] A similar analytical approach was used by Hirata *et al.* to describe density evolution in terms of dihedral angle and number of particle contacts.^[16] Kang proposed a pore filling theory explaining the redistribution of melt in liquid phase sintering. Driving force is the decrease of interface energy when smaller pores are filled with melt phase.^[17] For the final stage of liquid phase sintering, the author has proposed another thermodynamic model.^[18] It explains the formation of metastable states formed by segregation of liquid phase within the ceramic (Figure 1a). After adapting the sintering conditions according to the thermodynamic requirements a homogenous microstructure was achieved (Figure 1b). Weibull modulus was increased from 9 to 22, demonstrating the large effect of homogeneity on reliability of ceramics.^[19] The thermodynamic model was based on interface energy minimization in a two-phase solid-liquid system using a simple periodic microstructure.

A generalization of the model is presented in this paper. First, the thermodynamic criteria for inherently homogeneous sintering processes are explained. Then, a microstructure simulation is presented which can handle more complex geometry than the previous models. First results are presented showing parameters which affect formation of heterogeneous structures during sintering.

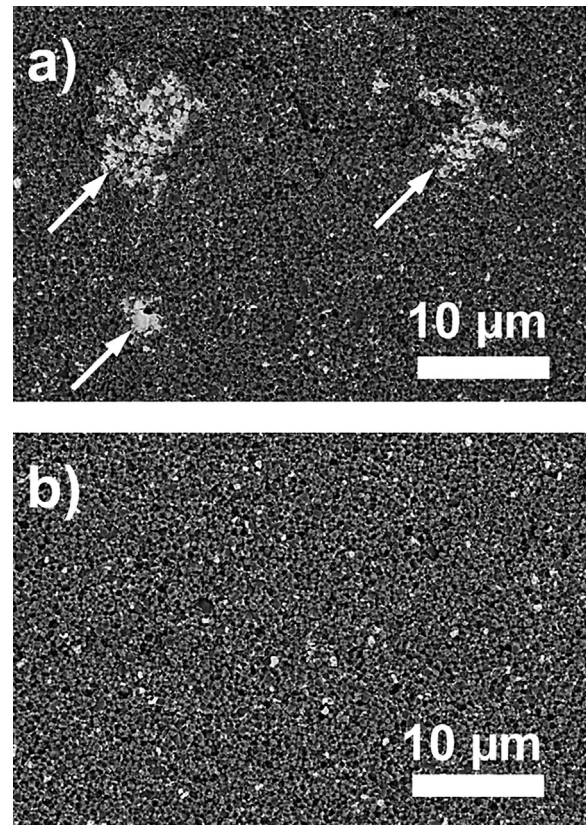


Fig. 1. Polished sections of liquid phase sintered aluminum nitride ceramics: a) before and b) after optimizing sintering parameters according to thermodynamic model (details in ref. ^[18,19]).

2. Thermodynamic Criteria

The driving force for sintering is the decrease in interface energy E_M of the sintered compact (index M denotes scaling with mass). Whereas interface energy before sintering is dominated by particle surfaces, grain boundary energy typically controls the interface energy in the final state. Figure 2 shows interface energy E_M versus specific volume v for a solid state sintering process. The specific volume is the inverse of the density ρ . It is used in Figure 2 instead of density because it simplifies the geometric construction of mixing energies (see below).

In the most general case, E_M is the sum of various contributions:

$$E_M(\rho) = \frac{\gamma_{sl} S_{sl}(\rho) + \gamma_{sg} S_{sg}(\rho) + \gamma_{lg} S_{lg}(\rho) + \gamma_{gb} S_{gb}(\rho)}{M}, \quad (2)$$

with M = mass, S = interface area, γ = specific interface energy and indices s , l , g , and gb denoting the solid, liquid, and gaseous phase and grain boundaries, respectively. In many systems, Equation 2 can be simplified as follows: with solid state sintering, S_{sl} and S_{lg} are zero; with viscous sintering, S_{gb} vanishes; and in the final state of liquid phase sintering, S_{sg} and S_{lg} can be neglected. On the other hand, specific interface

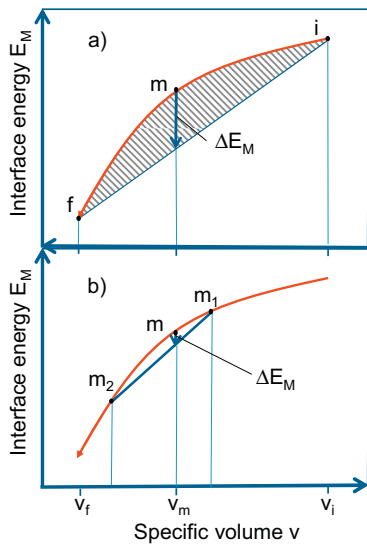


Fig. 2. a) Concave interface energy curve showing the energy gain ΔE_M by separation of dense and porous phase at average specific volume v_m and b) energy gain ΔE_M due to phase separation to intermediate states m_1 and m_2 .

energy γ may also change with sintering state and temperature: $\gamma = \gamma(\rho, T)$.^[20]

If the curve $E_M(\rho)$ has a concave shape – as indicated in Figure 2—the interface energy in an intermediate state of sintering can be decreased by a separation of denser and more porous regions. We consider a sintered body with an average specific volume v_m and assume that the mass in a volume V of this body is redistributed. In a partial volume V_i , the specific volume shall correspond to the initial value v_i and in the residual volume $V_f = V - V_i$, the specific volume shall correspond to the final value v_f . The mass fractions of the porous respectively dense regions are given by the so called lever rule,^[21] which simply reflects mass conservation:

$$\frac{M_i}{M} = \frac{v_m - v_f}{v_i - v_f}; \quad \frac{M_f}{M} = \frac{v_i - v_m}{v_i - v_f}. \quad (3)$$

The decrease of energy ΔE_M due to this phase separation is described by

$$\Delta E_M = E_{M_m} - \frac{(v_m - v_f)E_{M_i} + (v_i - v_m)E_{M_f}}{(v_i - v_f)} \quad (4)$$

with indices i, m , and f denoting the initial, intermediate, and final state of sintering, respectively. E_M, M , and v are the corresponding interface energies, masses, and specific volumes. ΔE_M is indicated in Figure 2a. It can be constructed by connecting the points i and f with a straight line and intersecting this line with the vertical line at v_m . Figure 2b demonstrates that any separation to other states than initial and final state also leads to a decrease of total energy if $E_M(\rho)$ is concave. The respective energy decrease ΔE_M can be calculated by Equation 4 as well or constructed graphically if

the initial and final states are replaced by the two intermediate states m_1 and m_2 with higher respectively lower specific volume. If interface energy is scaled with volume V instead of mass M , Equation 4 can be written in a similar way by replacing the specific volumes by densities or pore fractions. This representation has been selected in our previous publications.^[18,20] On the first view, this looks more convenient since specific volumes are rarely used in sintering science. But $E_V(\rho)$ does not represent a closed system with constant mass. Therefore, $dE_V(\rho)$ is not necessarily negative during sintering. To avoid confusion arising from increasing $E_V(\rho)$, the representation shown in Equation 4 is preferred. With liquid phase sintering, the specific volume can be used as well if phase separation between solid and liquid phase, on the one hand, and gaseous phase, on the other hand, shall be investigated. If phase separation between solid and fluid phases shall be discussed, the corresponding partial specific volume $v_s = V/M_s$ has to be used instead of v .

Note, that phase separation is well known from binary phase diagrams. If the free energy curves show concave sections, a miscibility gap exists.^[21] A homogenous mixture of two components is not stable in the concentration range of the miscibility gap. So, different phases coexist in the equilibrium state. Similarly, during sintering, the energy decrease ΔE_M resulting from a concave curve $E_M(\rho)$ creates a driving force for the separation of more or less dense regions in the intermediate stage. The driving force increases if the magnitude of the curvature rises. This must not necessarily lead to heterogeneities since densification can be faster than the separation process. Especially, a complete separation of initial and final state of sintering is not realistic. But, a concave interface energy curve always involves the risk of phase separation. Once these metastable heterogeneities are formed, it will be difficult to obtain a homogenous material in the final state, since many mechanisms – like grain growth – proceed differently in the respective regions. On the other hand, a straight or convex curve $E_M(\rho)$ does not bear such a risk as no thermodynamic driving force for the formation of heterogeneities during sintering exists. In that sense, inherently homogeneous sintering processes require convex or at least straight interface energy curves!

The thermodynamic driving force for the formation of heterogeneities during sintering – as described in the previous section – is considered essential for the evaluation of sintering processes. Therefore, it is necessary to introduce a measure which enables comparison of different sintering processes. The determination of interface energy with high enough accuracy and at small enough density intervals to allow for a satisfactory calculation of its curvature is very tedious. Instead it is suggested to use the area A between the curve $E_M(\rho)$ and the straight line connecting initial and final state, i.e., the dashed area in Figure 2a, as measure for the driving force for phase separation. Since phase separation and densification compete, area A should be scaled by the driving force for sintering. The latter is roughly represented by the slope s_l of the straight line connecting initial and final state of the

interface energy curve E_M :

$$D = -\frac{A}{s_i} = \frac{A(v_i - v_f)}{E_{M_i} - E_{M_f}} \quad (5)$$

D is denoted desintering parameter. A large D indicates a high risk of formation of heterogeneity during sintering, whereas a negative D characterizes an inherently homogeneous sintering process.

The desintering parameter D can be obtained experimentally or from computer simulation. For that, area A and density ρ respectively specific volume v have to be determined in the initial, intermediate and final stages of sintering. Experimentally this can be done using partially sintered and subsequently quenched specimen. From polished – and if necessary etched – sections of these specimens, interface areas S can be determined using SEM images and linear intercept analysis. The interface area S_{ij} between two phases is calculated from the number of intersections n_{ij} of the lines with the respective phase boundary and the total length L of the testing lines:^[22]

$$\frac{S_{ij}}{V} = \frac{2n_{ij}}{L} \quad (6)$$

with indices $ij = sl, sg, lg, \text{ or } gb$. The ratios between specific interface energies γ_{ij} are determined from measurements of dihedral angle and contact angle.^[23] Dihedral angles can be measured geometrically in SEM images of the polished sections and contact angles by heating microscopes.^[18] Density ρ is usually measured by Archimedes method. Using Equation 2, interface energy curve $E_M(\rho)$ is constructed at a number of discrete points. Then area A is obtained by numerical integration of this curve and finally the desintering parameter D is calculated according to Equation 5. Note that usually an unknown scaling factor remains in the determination of specific interface energies γ_{ij} . But this factor is eliminated when area A is divided by the slope s_i in Equation 5. Similarly, the desintering parameter D is obtained from microstructure models of the sintering process. With voxel-based models, artefacts due to the stepped interfaces can be avoided using the linear intercept method and orienting the test lines parallel to the coordinate axes.^[24]

In the following section, a voxel-based model is presented which allows the calculation of interface energies during sintering. For purposes of simplification, we concentrate on solid state sintering processes.

3. Microstructure Modeling

A voxel-based 3D representative volume element (RVE) was constructed using the in house software GeoVal.^[24] The work flow of the simulation is shown in Figure 3. It started with spherical particles. Typically 50 particles were used. The particles were placed in the RVE using a Poisson distribution generated by random numbers. An individual – small –

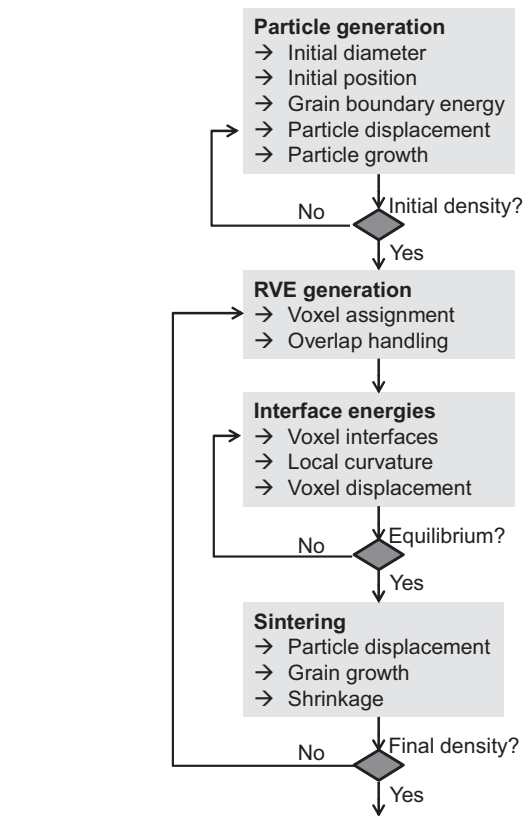


Fig. 3. Work flow during sintering simulation using deterministic model described in the text.

particle diameter was attributed to each particle obtained from a Gaussian distribution. Specific interface energies γ_{sg} were assigned to the particle surfaces and the grain boundaries γ_{gb} . Each particle was considered as a single crystal. The grain boundary energy between two individual particles i and j could be set according to a Gaussian distribution with the center γ_{gb} and a specified width. Usually the grain boundary energy γ_{gb} was constant.

The green microstructure was generated by a procedure roughly considering a wet forming process: all particle diameters were increased in small steps by the same scaling factor until particles touched. Particle centers were shifted according to hard sphere repulsion. The model was strictly periodic at the faces, edges and corners of the RVE. If particles were pushed out on one side of the RVE they were continued at the opposite side. If density was so high, that a displacement due to the hard sphere model was not possible any longer, the elastic energy corresponding to a Hertzian contact at the particle surfaces^[25] was minimized by further small displacements of the particle centers. Particle growth was stopped when a specified “green” density was achieved – typically 60%. The RVE was constructed by assigning each voxel to the corresponding particle or to the pore space respectively. If overlap between particles occurred voxels were attributed according to a Voronoi tessellation of the

overlap region. Particles with different radii were considered according to the radical plane technique.^[26] A typical size of the RVE was 64^3 voxels. Figure 4 shows a RVE at fractional density of 60% containing 50 spherical particles with a Gaussian distribution of diameters (1 ± 0.2) μm after rearrangement of particles according to hard sphere repulsion. The computer program ParaView has been used for graphical representation of the RVE.^[27] Note that smooth surfaces are intersections of the spherical particles with the faces of the RVE, whereas stepped structures reflect its porous interior.

During sintering, it was supposed that surface diffusion was much faster than grain boundary or volume diffusion as it was confirmed in many experimental studies.^[23] It was presumed that each particle surface had achieved a shape with minimal interface energy. To identify this equilibrium shape, local energy of voxels was determined in two steps. First, the voxel energy due to the next neighbors of each voxel was summed up. Second, the interface energy of each voxel was calculated considering the curvature and the voxel energy of the neighbor voxels up to the fourth neighbor shell. Whereas the first step corresponds to the procedure used in Monte Carlo simulations of sintering,^[28] the second step enables considering interface tension on a larger scale thereby smoothing the effects of the angular voxel structure. If grain boundaries occurred within the fourth neighbor shell, they were used for the calculation of local interface energy as well to enable the formation of realistic dihedral angles at the edges of sintering necks.

The energy decrease due to the redistribution of surface voxels was measured using the linear intercept method mentioned in the previous paragraph. If energy minimization had converged, a sintering step was performed. For that, forces between particles were determined from interface

tensions in the grain boundaries. These forces were summed up for each particle. Residual forces on the particle centers were used to calculate particle displacements for the next iteration step. Numerically, the displacements were performed in small steps using virtual springs connecting the particle centers until elastic energy had relaxed. From interface tensions in the grain boundaries, tensile and compressive stresses on the particles were also obtained. From these stresses, a parameter was derived which controlled individual grain growth or shrinkage of particles in the following iteration. If particle diameter was smaller than a tenth of mean diameter, the respective particle was removed. Thereafter, particle diameters were increased evenly until the set density of the next iteration step was obtained (Figure 3). The voxel dimensions were decreased accordingly to consider adequate shrinkage of the RVE and the interface energy was minimized again. The process was repeated until final density was achieved. Typically, a 1 or 2% increase in density was used in one iteration step. During all steps of the sintering simulation, the periodic continuation at the sides of the RVE was strictly observed. Note that diffusion processes are not implemented in the model. It provides simply a sequence of local interface equilibria.

The evaluation of the microstructure data has already been described in the previous paragraph. The whole process of particle generation and sintering was repeated typically 5 to 10 times to account for statistical effects. Figure 5 shows an example of microstructure evolution during sintering at a dihedral angle of 120° using the initial structure shown in Figure 4. Besides densification, coarsening of the microstructure is also observed.

4. Results and Discussion

The interface energy during sintering has already been investigated for periodic structures using triangular meshes.^[18] Interfaces with minimal energy were calculated by the computer program surface evolver,^[29] which had been intensively utilized by Wakai.^[30] To compare results obtained with the voxel model with results from the triangular mesh model, some simulations are presented below using a simple cubic arrangement of particles. Figure 6 shows particle shapes obtained with the voxel model for different dihedral angles of one truncated sphere located in the center of the cubic RVE. Size of the RVE was 64^3 voxels. Whereas a small dihedral angle leads to a convex particle shape, a large dihedral angle causes the expected mixture of convex and concave surfaces. The same structures were obtained using surface evolver (compare Figure 4 in ref.^[26]).

Figure 7 shows interface energy E_M versus specific volume during sintering of the simple cubic structure for a dihedral angle of 120° and different sizes of the RVE. Note that both quantities E_M and v were scaled by the respective values of the fully dense state. It can be seen that a fairly good convergence was already achieved for sizes between 16^3 and 32^3 voxels.

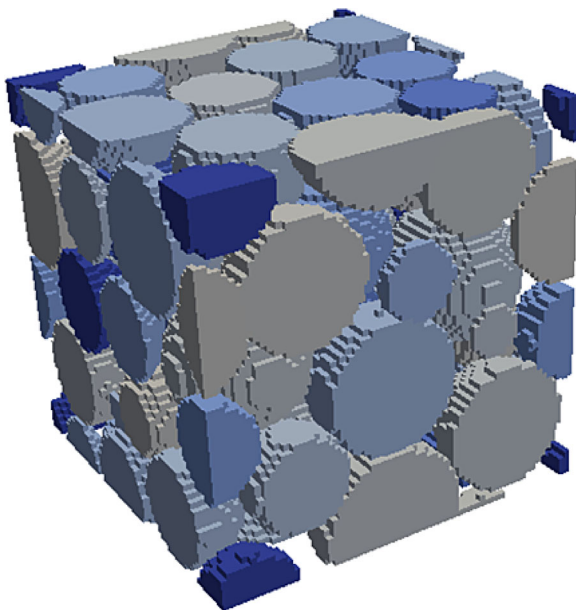


Fig. 4. RVE with 50 particles before sintering (fractional density 60%).

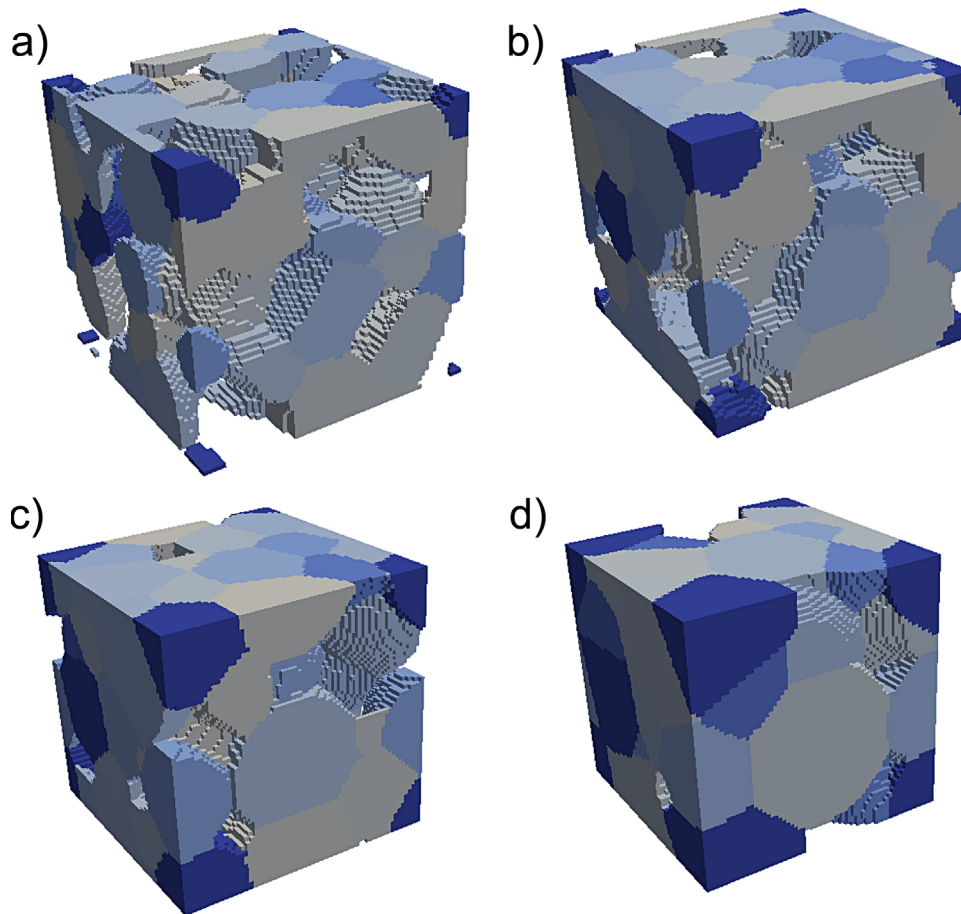


Fig. 5. RVE with 50 particles during sintering at different fractional densities: a) 60%, b) 70%, c) 80%, and d) 90%.

The effect of dihedral angle on the interface energy curves is shown in Figure 8 using RVEs with 64^3 voxels. The curves become steeper with increasing dihedral angle and curvature increases. This was already shown for simple cubic and face centered cubic structures using triangular meshes.^[20,18] Using triangular meshes, curvature of the interface energy curve

becomes slightly positive at dihedral angles smaller than 90° . In contrast, curvature is negative for all dihedral angles using the voxel model (compare Figure 8).

The difference is attributed to the coarser representation of the neck region in the voxel model which leads to inaccuracies especially at small dihedral angles. On the other hand, the

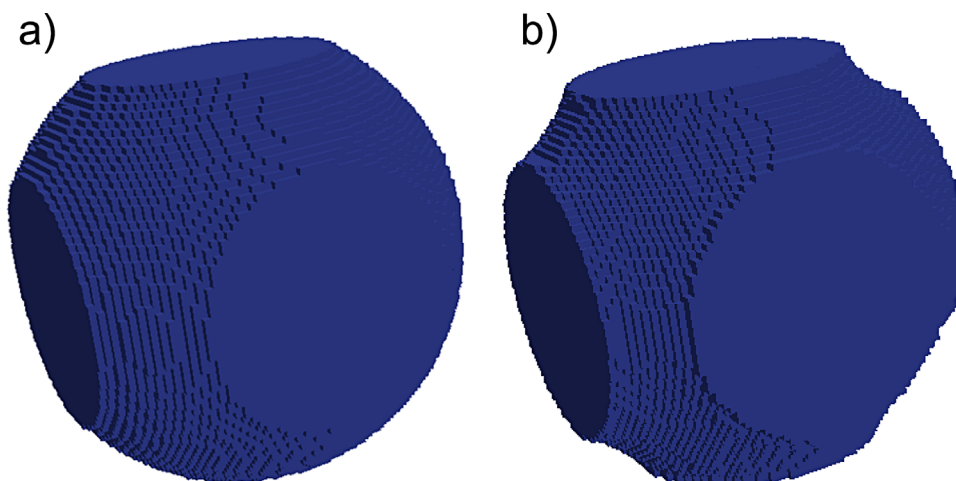


Fig. 6. Particles in a simple cubic arrangement at fractional density of 75% and dihedral angles of a) 60° and b) 150° .

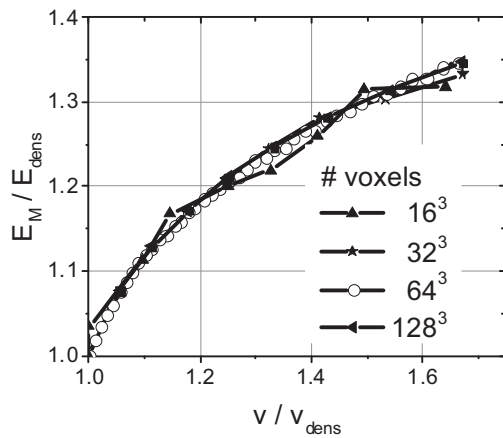


Fig. 7. Convergence of the cubic model at different sizes of the RVE.

voxel model allows the calculation of much larger models at reasonable computer times. Sintering of an RVE with 50 particles requires typically 1 or 2 h on a standard PC, whereas simulations using surface evolver are slower by about two orders of magnitude and stability of the algorithm is much worse. So, the voxel model is preferred for the simulation of complex structures. However, results with dihedral angles smaller than 90° obtained with the voxel model should be interpreted with care. The interface energy in the initial stage of sintering can also be compared with the Coble model using a dihedral angle of 180° , grain boundary diffusion and closed form equations.^[31] Interestingly, the Coble model provides a slightly convex interface energy versus specific density curve which is attributed to artefacts in the Coble model considering structures far away from local equilibrium.

Figure 9a shows interface energy curves for random arrangements of spherical particles sintered at different dihedral angles. Starting configurations in each case were several RVE containing truncated spheres. The particle diameters had a Gaussian distribution of $(1 \pm 0.2) \mu\text{m}$. An

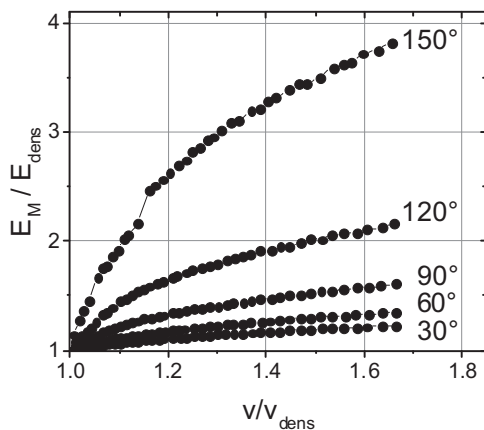


Fig. 8. Scaled interface energy E_M/E_{dens} versus scaled specific volume v/v_{dens} for simple cubic symmetry and different dihedral angles.

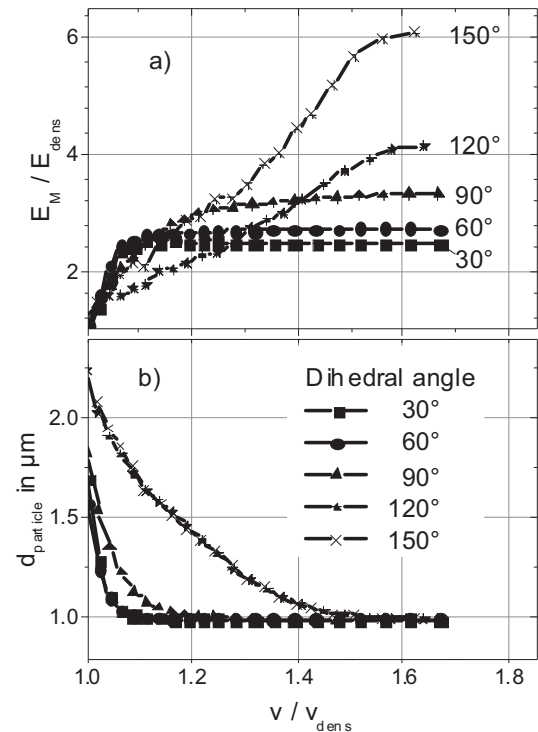


Fig. 9. a) Scaled interface energy E_M/E_{dens} versus scaled specific volume v/v_{dens} for RVEs with 50 spheres and different dihedral angles, b) evolution of particle diameters $d_{particle}$ during sintering.

example is shown in Figure 4. Moderate grain growth and particle displacement were allowed during sintering (compare Section 3). The interface energies are mean values from simulating 5 to 10 RVE per dihedral angle. The root mean squared errors are indicated in Figure 9a. They are hardly seen demonstrating high reproducibility of the simulation.

The good reproducibility is attributed to the periodic continuation at the sides of the RVE. Interface energy curves show concave shape at a dihedral angle of 90° and below. At higher dihedral angles, convex and concave regions of the curves occur (compare Figure 9a). The evolution of grain size during sintering is shown in Figure 9b. Moderate grain growth occurs for all dihedral angles. However, grain growth is significantly larger for large dihedral angles of 120° and 150° compared to dihedral angles of 90° and below. This increase is attributed to the larger grain boundary area which reduces the pinning of grain boundaries by pores. Figure 10 shows the desintering parameter (compare Equation 5) for the curves shown in Figure 9a. The desintering parameter significantly decreases at dihedral angles above 90° . This decrease corresponds to the lower curvature of interface energy curves in Figure 9a. Interestingly, the scaled variance also plotted in Figure 10 shows a similar decrease. This underlines the importance of the desintering parameter. It was not expected that disorder could be observed already on the scale of such small RVEs. Note that the thermodynamic criteria, presented in Section 2, do not allow conclusions on the size of the regions which are separated.

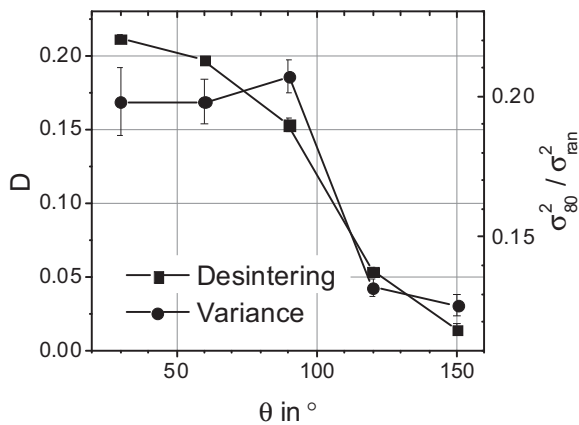


Fig. 10. Desintering parameter D (left axis) and scaled variance at fractional density of 80% σ_{80}/σ_{ran} (right axis) versus dihedral angle θ for the simulations shown in Figure 9.

Figure 11 shows the individual effects of surface diffusion and grain growth on the interface energy curves at a dihedral angle of 120° . Curvature is largest if neither surface diffusion nor grain growth occurs (curve A in Figure 11). Surface diffusion leads to a significant decrease of initial interface energy and a flattening of the interface energy curve (curve B in Figure 11). If grain growth is additionally switched on, the interface energy curve with concave and convex sections already shown in Figure 9a is obtained (curve C in Figure 11). Final interface energy decreases significantly compared to curve A and B. This is simply caused by the reduction of grain boundary energy with increase of grain size. Note that scaling was always done with the interface energy of dense RVEs obtained with grain growth. In addition also the effect of a distribution of grain boundary energies for individual grain boundaries was tested. But no effect on the interface energy curve was obtained.

Apparently, surface diffusion and grain growth can reduce the curvature of interface energy curves and thereby the

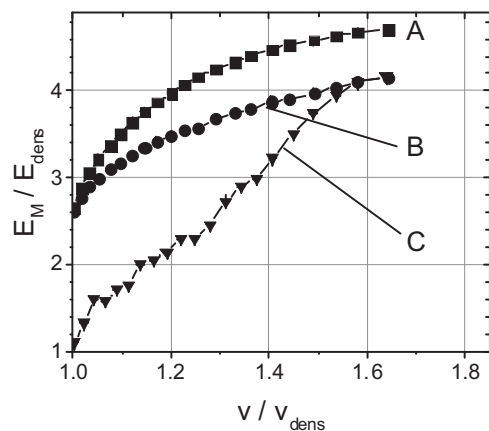


Fig. 11. Scaled interface energy E_M/E_{dens} versus scaled specific volume v/v_{dens} for RVEs with 50 spheres and dihedral angle of 120° for different combinations of grain growth and surface diffusion, curve A: no grain growth, no surface diffusion, curve B: no grain growth, surface diffusion, curve C: grain growth, surface diffusion.

tendency for differential sintering. This is an unexpected result especially for grain growth. For surface diffusion, the present results provide another explanation for the advantages of the above-mentioned precoarsening treatment suggested by De Jonghe.^[8] So, besides the mechanical stabilization of the microstructure, surface diffusion has a thermodynamic effect reducing the driving force for differential sintering. More differentiation is required to understand the effect of grain growth. Looking again at Figure 9b, it becomes clear that a drastic grain growth only in the final sintering stage – as it was obtained for small dihedral angles – has a detrimental effect since the final part of the interface energy curve is pulled down and becomes concave. Usually a late onset of grain growth is considered desirable in sintering studies, because final grain size can be reduced.^[23] The present paper suggests that grain size and microstructure homogeneity may be complementary in sintered systems. So, a tradeoff situation may exist where a moderate grain growth during the entire sintering cycle is helpful to improve reliability of sintered ceramics. One can speculate that some initial disorder is helpful to achieve this early onset of grain growth.

5. Conclusions and Outlook

Sintering involves billions of individual particles. Due to the statistical nature of many parameters affecting particle arrangement during forming, some heterogeneity will be inevitable. Heterogeneity can increase during sintering leading to large flaws in sintered compacts. These flaws deteriorate strength and reliability and have to be carefully avoided. To achieve better sintering processes, thermodynamic criteria should be considered. As shown in Section 2, the concave or convex shape of the interface energy curve during sintering provides a criterion whether a sintering process is inherently homogeneous. A desintering parameter has been derived which can be used to compare different sintering processes regarding their tendency for the formation of heterogeneous structures. The desintering parameter was calculated for a voxel-based model, already showing some parameters which are important in achieving inherently homogeneous sintering processes. Both surface diffusion and grain growth significantly affect the desintering parameter.

Besides the thermodynamic driving force, kinetic effects control the actual evolution of microstructure. Therefore, an evaluation of kinetic models with respect to the evolution of interface energy is required. Fortunately, many existing sintering models can be easily adapted to that purpose. Analytical sintering models are based on a simple geometry of the particle and pore geometry (compare, e.g., ref. ^[6,16]). They allow an easy extraction of interface energy but are restricted to sections of the sintering cycle. With the extension of Delannay, larger portions of the sintering cycle can be evaluated.^[32] Also, the geometric model of Wakai allows a simple extraction of surface energy.^[30] Obviously, the desintering parameter can be easily obtained from the Monte

Carlo models on sintering (compare, e.g., ref. [28]). In addition, it was pointed out in Section 2 that the desintering parameter can be derived experimentally using partially sintered samples. More investigations on the formation of heterogeneity during sintering are considered essential for the improvement of sintered material properties.

Received: October 27, 2014

Final Version: February 24, 2015

Published online: March 17, 2015

-
- [1] O. Sudre, F. F. Lange, *J. Am. Ceram. Soc.* **1992**, 75, 3241.
- [2] H. E. Exner, G. Petzow, *Adv. Sci. Technol.* **2006**, 45, 539.
- [3] P. Z. Cai, D. J. Green, G. L. Messing, *J. Am. Ceram. Soc.* **1997**, 80, 1940.
- [4] F. F. Lange, M. Metcalf, *J. Am. Ceram. Soc.* **1983**, 66, 398.
- [5] F. F. Lange, *J. Am. Ceram. Soc.* **1989**, 72, 3.
- [6] B. J. Kellet, F. F. Lange, *J. Am. Ceram. Soc.* **1989**, 72, 725.
- [7] F. F. Lange, B. J. Kellet, *J. Am. Ceram. Soc.* **1989**, 72, 735.
- [8] F. J. T. Lin, I. C. De Jonghe, *J. Am. Ceram. Soc.* **1997**, 80, 2269.
- [9] K. Maca, V. Pouchly, P. Zalud, *J. Eur. Ceram. Soc.* **2010**, 30, 583.
- [10] F. Raether, P. Schulze Horn, *J. Eur. Ceram. Soc.* **2009**, 29, 2225.
- [11] O. Lame, D. Bellet, M. Di Michiel, D. Bouvard, *Acta Mater.* **2004**, 52, 977.
- [12] Y. Yang, Thesis, Louisiana State University **2011**.
- [13] A. J. Pask, in *Sintering Key Papers* (Eds: S. Somiya, Y. Moriyoshi), Elsevier, Amsterdam **1990**, 567.
- [14] H. E. Exner, *Acta Metal.* **1987**, 35, 587.
- [15] F. Delannay, *Philos. Mag.* **2005**, 85, 3719.
- [16] Y. Hirata, A. Hara, I. A. Aksay, *Ceram. Int.* **2009**, 35, 2667.
- [17] Y.-P. Kim, S.-W. Jung, S.-J. L. Kang, *J. Am. Ceram. Soc.* **2005**, 88, 2106.
- [18] F. Raether, *Habilitation*, University of Wuerzburg, Germany **2009**.
- [19] A. Thimm, F. Raether, A. Klimera, J. Ruska, in Special Edition of CFI, *Ceram. Forum Int.: Thermal Process Engineering in the Ceramics Industry* (Eds: M. Herrmann, R. Clasen) **2008**, 24.
- [20] A. Klimera, F. Raether, J. Ruska, *J. Am. Ceram. Soc.* **2007**, 27, 1419.
- [21] A. D. Pelton, in *Phase Diagrams in Physical Metallurgy* (Eds: R. W. Cahn, P. Haasen), Elsevier, Amsterdam **1996**, 1, 472.
- [22] H. E. Exner, H. P. Hougardy, *Quantitative Image Analysis of Microstructures*, DGM Informationsgesellschaft Verlag, Oberursel, Germany **1988**.
- [23] M. N. Rahman, *Sintering of Ceramics*, CRC Press, Boca Raton, Florida **2008**.
- [24] T. M. Müller, F. Raether, *Comp. Mat. Sci.* **2014**, 81, 205.
- [25] H. Hertz, D. E. Jones, G. A. Schott, in *Miscellaneous Papers*, MacMillan, London **1896**.
- [26] M. Iuga, F. Raether, *Adv. Sci. Technol.* **2006**, 45, 89.
- [27] Software ParaView Version 4.2, www.paraview.org.
- [28] V. Tikare, M. Braginsky, D. Bouvard, A. Vagnon, *Comp. Mat. Sci.* **2010**, 48, 317.
- [29] K. Brakke, *Exper. Math.* **1992**, 1, 141.
- [30] F. Wakai, *J. Am. Ceram. Soc.* **2006**, 89, 1471.
- [31] R. L. Coble, *J. Am. Ceram. Soc.* **1958**, 41, 55.
- [32] F. Delannay, C. Colin, *Mater. Sci. Eng., A* **2008**, 495, 236.
-